UltraRapid Communication

Downregulation of Apoptosis-Inducing Factor in Harlequin Mutant Mice Sensitizes the Myocardium to Oxidative Stress–Related Cell Death and Pressure Overload–Induced Decompensation

Vanessa P.M. van Empel, Anne T. Bertrand, Roel van der Nagel, Sawa Kostin, Pieter A. Doevendans, Harry J. Crijns, Elly de Wit, Wim Sluiter, Susan L. Ackerman, Leon J. De Windt

Abstract—Apoptosis-inducing factor (AIF), or programmed cell death 8 (Pdcd8), is a highly conserved, ubiquitous flavoprotein localized in the mitochondrial intermembrane space. In vivo, AIF provides protection against neuronal apoptosis induced by oxidative stress. Conversely, in vitro, AIF has been demonstrated to have a proapoptotic role when, on induction of the mitochondrial death pathway, AIF translocates to the nucleus where it facilitates chromatin condensation and large scale DNA fragmentation. To determine the role of AIF in myocardial apoptotic processes, we examined cardiomyocytes from an AIF-deficient mouse mutant, Harlequin (*Hq*). *Hq* mutant cardiomyocytes demonstrated increased sensitivity to H_2O_2-induced cell death. Further, *Hq* hearts subjected to ischemia/reperfusion revealed more cardiac damage and, unlike wild-type mice, the amount of damage increased with the age of the animal. Aortic banding caused enhanced hypertrophy, increased cardiomyocyte apoptotic and necrotic cell death, and accelerated progression toward maladaptive left ventricular remodeling in *Hq* mutant mice compared with wild-type counterparts. These findings correlated with a reduced capacity of subsarcolemmal mitochondria from *Hq* mutant hearts to scavenge free radicals. Together, these data demonstrate a critical role for AIF as a cardiac antioxidant in the protection against oxidative stress–induced cell death and development of heart failure induced by pressure overload. **(*Circ Res*. 2005;96:e92–e101.)**

Key Words: apoptosis ■ heart failure ■ oxidative stress ■ apoptosis-inducing factor

Heart failure, a prevalent cause of morbidity and mortality worldwide, proceeds through a common process termed cardiac remodeling in which heart chambers become markedly enlarged and contractile function deteriorates.[1] Recent insight from animal models and human end-stage heart failure material have identified a roughly 8- to 25-fold increase in the levels of myocyte apoptosis over that observed in healthy tissue. Studies in genetic mouse models that mimic this situation suggest that chronic elevation of myocyte apoptosis may constitute a causal component in the cardiac remodeling process preceding heart failure.[2]

Two major apoptotic pathways are operative in mammalian cells, including the cardiac muscle cell. Mitochondria play a key role as apoptosis occurs through the opening of the mitochondrial permeability transition pore,[3] the release of cytochrome c, assembly of the apoptosome, and subsequent activation of downstream caspase-9 and -3.[4,5] Secondly, the death-receptor pathway is triggered by binding of members of the death-receptor superfamily, such as Fas or CD95 and TNF-α, to their cognate receptors, which induces receptor clustering, formation of a death-inducing signaling complex, and finally, caspase-8 and -3 activation.[6–8] Downstream of caspase-3, the apoptotic program branches into a multitude of subprograms, such as the activation of ICAD-CAD which serves to cleave essential cardiac structures, including actin, alpha-actinin, lamin, and serum response factor.[9–12]

Apoptosis-inducing factor (AIF), also known as programmed cell death 8 (Pdcd8), is a highly conserved flavoprotein with pyridine nucleotide-disulphide oxidoreductase and DNA binding domains. The AIF precursor is synthesized in the cytosol and imported into mitochondria, where AIF localizes, like cytochrome c, in the mitochondrial intermembrane space in healthy cells. Changes in mitochondrial permeability, secondary to loss of the mitochondrial mem-

Original received June 22, 2004; first resubmission received November 16, 2004; second resubmission received May 3, 2005; revised second resubmission May 19, 2005; accepted May 19, 2005.

From the Hubrecht Laboratory and Interuniversity Cardiology Institute Netherlands (V.P.M.v.E., A.T.B., R.v.d.N., L.J.D.W.), Royal Netherlands Academy of Arts and Sciences, Utrecht, the Netherlands; Max-Planck-Institute (S.K.), Bad Nauheim, Germany; Heart Lung Center Utrecht (P.A.D.), the Netherlands; Department of Cardiology (H.J.C.), University Hospital Maastricht, the Netherlands; Department of Biochemistry (E.d.W., W.S.), Erasmus MC, Rotterdam, the Netherlands; and The Jackson Laboratory (S.L.A.), Bar Harbor, Maine.

Correspondence to Dr Leon J. De Windt, Hubrecht Laboratory and Interuniversity Cardiology Institute Netherlands, Royal Netherlands Academy of Arts and Sciences, Uppsalalaan 8, 3584 CT Utrecht, the Netherlands. E-mail dewindt@niob.knaw.nl

Circulation Research **is available at http://circres.ahajournals.org** **DOI: 10.1161/01.RES.0000172081.30327.28**

brane potential ($\Delta\Psi_m$), induce translocation of the mature form of AIF, lacking NH_2-terminal mitochondrial localization signals, through the mitochondrial permeability transition pore into the cytosol and nucleus, where its DNA binding activity is thought to facilitate chromatin condensation and large scale DNA fragmentation.[13]

An additional role for AIF in cell survival was uncovered in the *Hq* mutant mouse, which displays progressive degeneration of cerebellar and retinal neurons because of a proviral insertion into the first intron of the *aif* gene, leading to an 80% decrement in AIF expression.[14] Cerebellar granule cells from *Hq* mutant mice were more susceptible to hydrogen peroxide–induced cell death, whereas retroviral reintroduction of wild-type (WT) AIF rescued mutant cells, suggesting that AIF can protect against oxidative stress–related cell death.[14] In summary, the combined observations suggest that AIF may fulfill a dual role in cellular homeostasis: a prosurvival function when localized in the mitochondrial intermembrane space likely via its oxidoreductase activity; and an apoptogenic action once in the nucleus depending on its DNA-binding ability and association with Endo G.[15,16]

Presently, the role of AIF in myocardial apoptosis or cell survival is unknown. To this end, we examined cardiomyocytes isolated from the *aif* hypomorphic mutant, *Hq*. These AIF-deficient myocytes were found to be sensitized to oxidative stress–induced cell death, and *Hq* hearts revealed more ischemic damage and larger infarct size after acute ischemia/reperfusion, with the extent of damage worsening with age. *Hq* mice subjected to chronic stress in the form of pressure overload elicited accelerated maladaptive left ventricular remodeling and signs of heart failure. Finally, *Hq* mitochondria displayed a 29% decrease in their ability to neutralize exogenously provided H_2O_2, which is consistent with a role for AIF as a pivotal mitochondrial free radical scavenger in the heart. Our findings underscore the premise that, similar to neuronal cells, AIF enhances survival of cardiac muscle cells via its ability to protect the myocardium against oxidative stress–induced cell death.

Materials and Methods

Mice

WT male and female mice on a B6CBACa-$A^{w\text{-}J}/A$ (B6CBA) background and mice hemizygous or homozygous for the X-linked harlequin mutation ($Pdcd8^{Hq}$; *Hq*) on the same background were used (The Jackson Laboratory, Bar Harbor, Me). Muscle LIM Protein (MLP)-deficient[17] and WT mice in a 129/Sv background, were generously provided by Howard A. Rockman (Duke University Medical Center, Durham, NC). All protocols were performed according to institutional guidelines and were approved by local Animal Care and Use Committees.

Cardiomyocyte Cultures and siRNA Transfection

Neonatal rat ventricular myocytes were obtained as described previously in detail.[18] Neonatal ventricular mouse myocytes were obtained by enzymatic dissociation of 1- to 2-day old B6CBA or B6CBA:$Pdcd8^{Hq}$ neonatal ventricles. Ventricles were stored in HEPES buffered DMEM (pH 7.4) before multiple rounds of enzymatic digestion in DMEM nutrient mixture F-12 Ham base (Sigma) supplemented with 0.7 mg/mL collagenase type 2 (Invitrogen) and 1 mg/mL pancreatin (Sigma). Cells were collected by centrifugation at 61*g* for 10 minutes, resuspended in neonatal calf serum (Invitrogen), and stored in an incubator at 37°C. All cell suspensions were pooled, centrifuged at 61*g* for 10 minutes, and resuspended in DMEM (Invitrogen) supplemented with 10% horse serum (Invitrogen) and 5% fetal calf serum (Invitrogen). Subsequently, the cells were differentially plated for 3 hours in uncoated cell culture dishes to remove contaminating nonmyocytes. The cardiomyocytes (containing <5% nonmyocytes) were then plated on fibronectin-coated 6-well culture dishes (Sigma). Approximately 24 hours after plating the media was replaced by DMEM:M199 (4:1) medium (serum-free medium). For siRNA transfection, neonatal mouse cardiomyocytes were plated in DMEM supplemented with Nutridoma (Roche) in 12-well fibronectin-coated plates with density of 4×10^5 cells per well and transfected the next day with 100 nM of siRNA duplex (Ambion) specific for GFP ("siRNA-control" 5′-AACGAUGCCACCUACGGCAAGdTdT-3′) or a duplex specific for murine AIF ("siRNA-AIF" 5′-GGCUCAGUUCCUCAGAUCAdTdT-3′) in 2 μL oligofectamine (Invitrogen). Cells were washed the next day and incubated for another 48 hours before treatment.

Quantification of Cell Death in Cell Culture

Cell death was assessed by double-staining neonatal mouse cultures with propidium iodide (PI; 2.5 μg/mL, Molecular Probes) and Hoechst 33258 (2 μg/μL).

Ischemia-Reperfusion and Measurements of Ischemic Area at Risk and Infarct Size

Two- and 6-month-old WT and *Hq* mice were randomized to receive either ischemia-reperfusion injury or a sham procedure. Mice were anesthetized with isoflurane and placed on a warming pad maintained at 37°C. The trachea was cannulated with a polyethylene tube connected to a respirator (Harvard Apparatus) with a tidal volume of 0.6 mL (110/min). A left lateral thoracotomy was performed between the fourth and fifth ribs, pericardial tissue was removed, and the left anterior descending artery (LAD) was visualized and ligated with a slipknot of 8-0 silk. Reperfusion was initiated 30 minutes after the occlusion. After reperfusion, mice were anesthetized, the LADs were reoccluded, and 1 mL of 1.0% Evans blue was injected into the apex of each heart to stain nonischemic tissue. The hearts were then excised, washed with PBS, and cut into 5 transverse slices for 15 minutes of incubation at room temperature with 1.5% 2,3,5-triphenyltetrazolium chloride (TTC) to measure viable myocardium (red staining). Slices were photographed (each side) under a microscope and left ventricular area, area-at-risk (AAR), and infarct area (IA) were determined by digital planimetry.

Aortic Banding

Transverse aortic banding (TAC) or sham surgery was performed in 4-month-old B6CBA or B6CBA:$Pdcd8^{Hq}$ mice and in the MLP WT 129/Sv strain. The aorta was subjected to a defined 25-gauge constriction between the first and second truncus of the aortic arch as described.[19,20]

Western Blot Analysis

Immunoblot analysis was performed as described previously in detail.[18] Specifically, anti-AIF (sc-9416, Santa Cruz), anti-MnSOD (106-984, Upstate), and anti-GAPDH (MAP 378, Chemicon) antibodies were used. Immunoreactivity was detected with Chemiluminescence (ECL, Amersham Pharmacia Biotech).

Transthoracic Echocardiography

Echocardiographic measurements were performed on mice anesthetized with isoflurane as described.[21] In M-mode, the following parameters were obtained: end diastolic left ventricular (LV) internal diameter (LVIDd), end-systolic LV internal diameter (LVIDs), and posterior wall (PW) and interventricular septum (IVS) wall thickness. Fractional shortening (FS) was calculated as (LVIDd−LVIDs)/LVIDd×100, echocardiographic LV mass (mg) was calculated by use of an uncorrected cube assumption as LV mass=[(LVIDd+LVPWd+ IVSd)^3−(LVIDd)^3](1000). Doppler echocardiography was used to calculate the pressure gradient between the proximal and distal sites of the transverse aortic constriction using the Doppler-

estimated Bernoulli equation,[22] and only mice with a pressure gradient >20 mm Hg were used in this study.

Immunolabeling, Immunofluorescence, and Confocal Microscopy

Heart tissue was fixed in 3.7% formaldehyde, embedded in paraffin, and sectioned at 6-μm thickness for visualization. Sections were stained with hematoxylin and eosin (H&E), or Sirius red, or incubated with antibodies against cleaved caspase-3 (1:1000; Cell Signaling) or cleaved PARP (1:200; Cell Signaling). Envision+ kit (DAKO) was used as a secondary reagent. Stainings were developed using DAB (brown precipitate), and slides were counterstained with hematoxylin and visualized using a Nikon Eclipse E600 microscope. TUNEL and anticomplement 9 stainings were performed on 10-μm cryosections as described previously in detail[23] using a TMR red TUNEL kit (Roche) or an anti–NCL-CCC9 antibody (1:50; Novocastra), respectively. Double staining was performed with anti–phalloidin-FITC (1:500; Sigma), DRAQ5 (1:1000; Alexis), and/or DAPI (1:500; Molecular Probes). The samples were examined with a confocal scanning laser microscope Leica TCSNT, equipped with argon/krypton and helium/neon lasers.

In Situ Detection of Reactive Oxygen Species

Reactive oxygen species (ROS) production was determined using the fluorescent dye dihydroethidium (DHE). Cryosections (10 μm) were incubated with 5 μm DHE at 37°C for 30 minutes. Images were captured on a Zeiss Axiovert 135 mol/L microscope and pixel intensity of the nuclei measured using SPOT-advanced software.

Measurement of Mitochondrial Complex and H_2O_2 Scavenging Function

Snap-frozen hearts were re-thawed on ice, minced in a small volume of buffer sucrose medium (250 mmol/L sucrose; 10 mmol/L HEPES, pH 7.4; 1 mmol/L EDTA), and homogenized. Citrate synthase activity of the homogenate, expressed in mU as nmol 5-thio-2-nitrobenzoate (TNB)/min per mg protein, was measured by monitoring the CoA-coupled conversion of Ellman reagent into TNB at 412 nm.[24] The complex I activity, expressed in mU as nmol NADH/min per mg protein, was measured according to Birch–Manchin and Turnball[25] after freeze-thawing the homogenate 3 times with the following modifications: before initiating the reaction, the sample in the reference cuvette was incubated for 1 minute in the presence of 3.5 mmol/L rotenone to allot sufficient time for its binding to the enzyme complex. The reaction was initiated by the addition of CoQ_1 to the sample and reference cuvette and registered as the rotenone-sensitive NADH:ubiquinone oxidoreductase activity by following the decrease in absorbance at 340 nm with 380 nm as the reference wavelength. The assay of complex IV activity of the homogenate was adapted from Birch–Machin and Turnball's method.[25] The initial rate of oxidation of cytochrome C at 37°C was followed at 550 nm using 540 nm as the reference wavelength and expressed in mU as nmol oxidized cytochrome C/min per mg protein. Cytochrome C was reduced with sodium dithionite and purified by gelfiltration on a Sephadex G-25 Medium column (PD-10).

For H_2O_2 scavenging function, subsarcolemmal mitochondria were freshly isolated as described previously.[26] Hydrogen peroxide (H_20_2) clearance rate was measured following the decrease in absorbance rate at 240 nm for 20 sec after administration of 10.5 mmol/L H_2O_2 in 50 mmol/L phosphate buffer (pH 7.0).[27]

Statistical Analysis

The results are presented as means±SEM. Statistical analyses were performed using INSTAT 3.0 software (GraphPad) and Student *t* test or ANOVA followed by Tukey posttest when appropriate. Statistical significance was accepted at a *P* value <0.05.

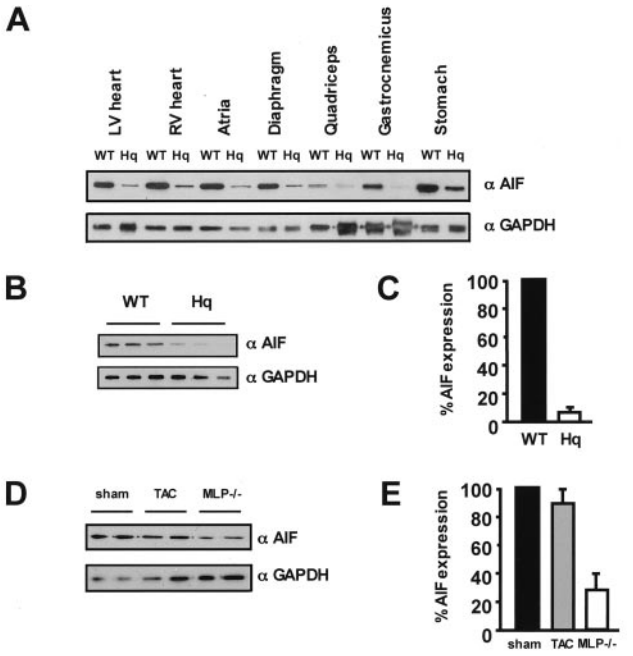

Figure 1. AIF expression in muscle (A) AIF protein levels (upper) were analyzed as described in Methods section in cardiac, skeletal, and smooth muscle (10 μg loading per lane) isolated from WT and *Hq* mice. Abundant presence of AIF in cardiac and smooth muscle was observed in WT mice, and substantial lower AIF expression in each corresponding muscle type in the *Hq* model. Membranes were reprobed for GAPDH as loading controls (lower). B, AIF (upper) and corresponding GAPDH protein expression (lower) in LV heart muscle (10 μg loading per lane) from WT and *Hq* mice. C, Quantification indicates that AIF protein expression in the AIF hypomorphic *Hq* mouse amounts to 8±2% of WT mice. D, AIF expression (10 μg loading per lane) slightly decreases on TAC, and is substantially downregulated in heart failure (MLP-deficient mouse). E, Quantification indicates that AIF cardiac protein expression amounts to 90±5% in TAC and 28±5% in heart failure (MLP−/−) mice.

Results

AIF Downregulation Sensitizes Cardiomyocytes to Oxidative Stress

As a first step in exploring the function of AIF in cardiac muscle cells, we determined its relative abundance in 3 major muscle types by Western blot analysis, revealing abundant presence of AIF protein in cardiac and smooth muscle, and, to a lesser extent, in skeletal muscle (Figure 1A). It is established that AIF also redistributes from mitochondria to cytosolic and nuclear fractions in cardiac myocytes on apoptotic stimuli,[28,29] but the function of AIF in the heart has not been directly addressed. To address the functional significance of AIF in normal and diseased cardiac muscle, we used a hypomorphic AIF mouse mutant, Harlequin (*Hq*). We first scrutinized whether *Hq* mice display myocardial or vascular abnormalities at baseline. *Hq* mice displayed no discernable cardiovascular phenotypes, apart from an increase in the heart weight (HW) to bodyweight ratio, because of reduced body fat deposition in the mutants (data not shown). HW to tibia length ratio was similar to those of WT mice, indicating the absence of cardiac hypertrophy, and *Hq* mice displayed normal cardiac function as assessed by echocardiography (Table and data not shown). Extended blood analyses showed

Echocardiographical Characteristics in WT and *Hq* Mice after Sham Operation and After Transverse Aortic Constriction

	Sham		7 Days After TAC		14 Days After TAC		28 Days After TAC	
	WT	*Hq*	WT	*Hq*	WT	*Hq*	WT	*Hq*
n	4	5	10	14	10	10	7	6
HR	462±21	388±45	439±14	372±20	456±12	380±18	456.0±12.4	379.8±17.5
IVSd, mm	0.93±0.10	1.01±0.10	1.05±0.04	1.21±0.06	1.15±0.06	1.25±0.06	1.27±0.03	1.20±0.06
IVSs, mm	1.53±0.05	1.64±0.16	1.75±0.05	1.68±0.07	1.76±0.08	1.68±0.108	1.58±0.06	1.34±0.06
LVPWd, mm	1.12±0.08	1.11±0.06	1.18±0.05	1.28±0.06	1.38±0.06	1.44±0.06	1.65±0.07*	1.61±0.05*
LVPWs, mm	1.54±0.07	1.56±0.05	1.59±0.09	1.66±0.06	1.84±0.06	1.80±0.06	1.97±0.08*	1.91±0.05*
LVIDd, mm	2.56±0.22	2.62±0.27	2.44±0.15	2.60±0.09	3.04±0.09	3.11±0.09	3.00±0.11	3.06±0.10
LVIDs, mm	1.03±0.08	1.02±0.08	0.90±0.07	1.37±0.05*†	1.47±0.04*	1.97±0.04*†	1.70±0.05*	2.12±0.09*†
%FS	59.8±1.2	60.7±1.2	63.7±1.9	47.1±1.0*†	51.5±1.7*	36.8±1.7*†	43.0±0.9*	30.8±1.0*†
Lvmass, mg	82±1	89±2	91±1	117±2	146±2*	169±3*	180±3*	206±4*†
AoPg, mm Hg	6±1	6±1	24±3*	23±3				

Data are expressed as means±SEM. WT indicates wild-type; *Hq*, harlequin; PWthd, posterior wall thickness in diastole; PWths, posterior wall thickness in systole; LVIDd, left ventricular internal diameter in diastole; LVIDs, left ventricular internal diameter systole; FS, left ventricular internal diameter in systole; FS, left ventricular fractional shortening calculated as (LVIDd-LVIDs)/LVIDd; AoPg, aortic pressure gradient; echocardiographic LV mass.

*$P<0.05$ vs corresponding sham group; †$P<0.05$ vs WT in same after TAC group.

no signs of anemia or structural abnormalities, except for a minor increase in white blood cell count (supplemental Table I, available at http://circres.ahajournals.org). In line with previous findings,[14] AIF expression was substantially downregulated in all major muscle types, as evidenced by Western blot analysis (Figure 1A). The amount of AIF expression in LV heart muscle of *Hq* mice was found to be 8%±2% compared with their WT counterparts (Figure 1B and 1C). To address whether AIF levels fluctuate in hypertrophy and heart failure, Western blots were performed on cardiac tissue from control mice, mice subjected for 1 week to TAC, and in the heart failure MLP-deficient mouse model (Figure 1D and 1E). Compared with control mice, AIF protein amounted to 90%±5% after TAC and only to 28%±5% in the MLP-deficient heart failure model, indicating that with increasing severity of hypertrophy/heart failure, cardiac AIF expression decreases.

If a proapoptogenic function of AIF would prevail in the heart, a loss of function mutation for AIF would prevent cardiac muscle from going into apoptosis elicited by noxious stimuli. Conversely, if AIF would function to protect myocytes against oxidative stress–mediated cell death, as described for *Hq* mutant cerebellar granule cells,[14] *Hq* myocytes would reveal a higher susceptibility to peroxide-mediated cell death. To this end, primary cardiomyocyte cultures derived from neonatal *Hq* and WT mice were analyzed under SF conditions or exposed to increasing doses of H_2O_2 (100 and 500 μmol/L) for 24 hours, followed by PI staining to identify myocyte apoptosis. Significantly more cell death was observed in AIF-deficient cardiomyocytes treated with 500 μmol/L H_2O_2 compared with WT cardiomyocytes (24.8%±1.3% and 17.4%±1.7% PI-positive cells, respectively; $P<0.05$; Figure 2A). This effect was abrogated when cultures were pretreated with EUK-8, an antioxidant with superoxide dismutase (SOD), catalase, and oxyradical scavenging properties (WT, 9.4%±1.1%; *Hq*, 8.0%±0.1%; $P<0.05$; Figure 2A). In contrast, AIF deficient myocytes were equally sensitive as WT myocytes to varying doses of other cell death inducers such as staurosporin (1.0 and 2.0 μmol/L) or etoposide (50 and 100 μmol/L; Figure 2B and 2C), and, notably, administration of EUK-8 had no effect on staurosporin- or etoposide-induced cell death in *Hq* or WT myocytes (Figure 2B and 2C).

Next, AIF expression was suppressed in WT mouse cardiomyocytes by siRNA transfection, and cell death was scored by PI staining after control or 500 μmol/L H_2O_2 treatment. The extent of AIF downregulation achieved amounted to 85%±3% (Figure 2D), which was comparable to the level of downregulation in *Hq* myocytes (Figure 1B and 1C). Mock-transfected cardiomyocytes, myocytes transfected with a control siRNA, and AIF-siRNA transfected myocytes had low and similar levels of cell death under SF conditions (Figure 2E). Conversely, significantly more cell death was observed in AIF-siRNA transfected cardiomyocytes treated with 500 μmol/L H_2O_2 compared with mock transfected or control-siRNA transfected cardiomyocytes (mock 19.3%±2.8%, control-siRNA 18.1%±1.7%, AIF-siRNA 29.1%±2.7% PI-positive cells, respectively; $P<0.05$; Figure 2E). Collectively, these data suggest that AIF deficiency renders cultured cardiomyocytes specifically more susceptible to oxidative stress–induced cell death.

AIF Deficiency Sensitizes the Heart to Ischemia/Reperfusion Damage

To more thoroughly evaluate the correlation between AIF, oxidative stress, and cardiac cell death, we analyzed cohorts of *Hq* and WT mice for their susceptibility to ischemia-reperfusion injury. Two- and 6-month-old male and female *Hq* mice and age-, sex-, and strain-matched WT controls were initially subjected to 30 minutes of occlusion of the LAD followed by 4 or 24 hours of reperfusion. Whereas WT mice survived this protocol, >80% of *Hq* mutant mice succumbed during the first hours of reperfusion, most likely because of lethal ventricular arrhythmias (data not shown), which forced

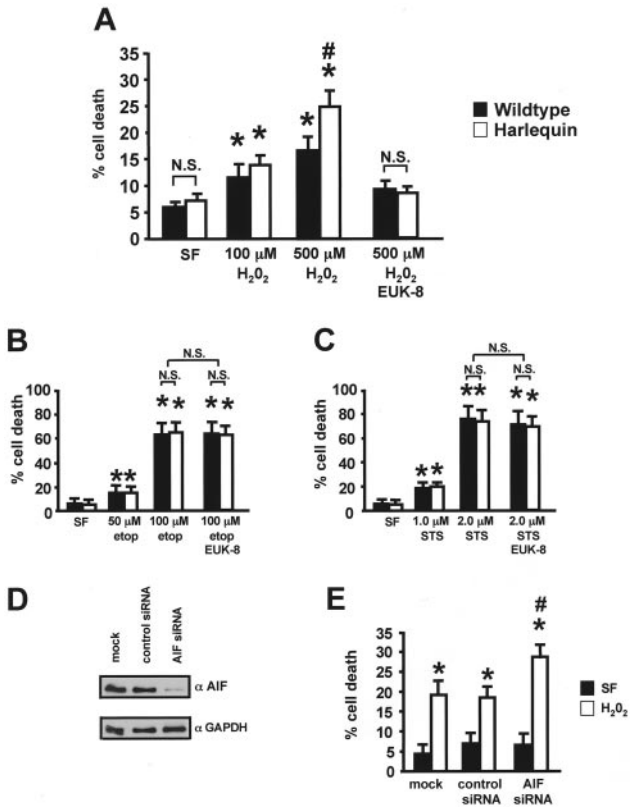

Figure 2. Increased cell death in AIF deficient mouse cardiomyocytes after oxidative stress. A, *Hq* and WT mouse myocytes were cultured under SF conditions or exposed to 100 or 500 μmol/L H_2O_2 for 24 hours, with or without EUK-8, an antioxidant, and subjected to PI/Hoechst 33342 costaining and scored for PI-positivity. *Hq* cardiomyocytes showed a tendency toward more cell death after 100 μmol/L H_2O_2 compared with WT cardiomyocytes treated with 100 μmol/L H_2O_2 (N.S.), and this became significant with the higher dose of 500 μmol/L H_2O_2 ($P<0.05$; n=3). This effect was abrogated when EUK-8 was added. B, No difference in cell death was observed between WT and mutant cardiomyocytes treated with increasing doses of etoposide or (C) staurosporin (STS) for 24 hours (n=3). Addition of EUK-8 had no effect on etoposide or STS-induced cell death in WT and *Hq* myocytes. Cells were stained with PI and Hoechst 33342 and scored for PI positivity as described above. *$P<0.05$ *Hq* vs WT. D, Suppression of AIF expression by siRNA. Cells were mock-transfected or transfected with a control siRNA or an AIF-specific siRNA, and the abundance of AIF was determined by immunoblot 48 hours later (upper) and reprobed for GAPDH as a loading control (lower; 5 μg loading per lane). E, Mouse myocytes were mock transfected, transfected with a control siRNA or AIF-siRNA, and either or not exposed to 500 μmol/L H_2O_2 for 24 hours, subjected to PI/Hoechst 33342 costaining, and scored for PI-positivity. AIF-siRNA transfected cardiomyocytes demonstrated significantly more cell death after 500 μmol/L H_2O_2 compared with mock- or control-siRNA transfected cardiomyocytes treated with 500 μmol/L H_2O_2 ($P<0.05$; n=3).

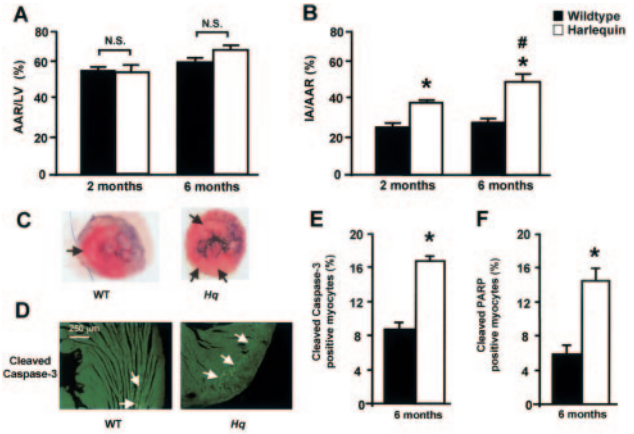

Figure 3. AIF-deficient mice demonstrate an increased infarct size. A, AAR, expressed as percentage of total LV, was comparable in *Hq* and WT mice at 2 and 6 months of age, indicating that no genotype-dependent differences existed in the perfused areas. B, Infarct size after 30 minutes of LAD occlusion, followed by 60 minutes of reperfusion in 2- and 6-month-old Harlequin and WT mice. The IA/AAR ratio was significantly higher in *Hq* mice compared with WT mice at 2 months (n=8). Furthermore, this ratio increased even further in 6-month-old *Hq* mutants, but not in WT mice ($P<0.05$; n=8). C, Representative images of 2-month-old WT and *Hq* mutant hearts stained with Evan's blue/TTC after 30 minutes of ischemia and 60 minutes of reperfusion. Note that in the *Hq* mutant heart the pale white infarct area (arrows) extends further within the AAR and is significantly larger than in the WT heart (* indicates $P<0.05$ *Hq* vs WT; #$P<0.05$ 2-month vs 6-month-old; n=4 to 6 for each group). D and E, 6-month-old WT and *Hq* hearts subjected to ischemia/reperfusion (I/R), stained for activated (cleaved) caspase-3, displayed more caspase-3 positive cells within the remaining region of viable left ventricle and septum in *Hq* hearts compared with their WT counterparts. Arrows indicate LV regions of caspase-3 positivity (n=3). F, *Hq* hearts subjected to I/R demonstrated increased cleaved PARP positive myocytes compared with the WT controls (n=3). *$P<0.05$ *Hq* vs WT.

us to reduce the reperfusion time to 1 hour while maintaining the animals under continuing anesthesia. After this 1-hour reperfusion period, the LAD was religated and hearts were perfused with Evans blue dye, removed, and incubated in TTC to quantify AAR and IA, respectively. The AAR/total LV area ratio did not differ between 2- and 6-month-old mutant and WT mice (2 months: WT, 53.4%±1.7%; *Hq*, 52.7%±3.6% N.S.; 6 months: WT, 57.9%±2.0%; *Hq* 64.3%±2.0%; N.S.; Figure 3A), indicating that there were no genotype-dependent differences in the perfused areas between the experimental groups. In contrast, the infarct area was increased by 50% in 2-month-old mutant mice (IA/AAR: WT, 23.9%±1.8%; *Hq* mice, 36.8%±1.2%; $P<0.05$, Figure 3B) and by 78% in 6-month-old *Hq* mice compared with their WT counterparts (IA/AAR: WT 26.6%±1.5%; *Hq*, 47.4%±3.4%; $P<0.05$; Figure 3B and 3C).

The increase in infarct area coincided with an elevated level of apoptotic cell death within the remaining region of viable left ventricle and septum of *Hq* mice, as evidenced by increased levels of myocytes positive for cleaved caspase-3 (WT: 8.7%±0.7%; *Hq*: 16.7%±0.6%; $P<0.05$; Figure 3D and 3E), myocytes positive for cleaved PARP (WT: 5.6%±1.1%; *Hq*: 14.4%±1.0%; $P<0.05$; Figure 3F), and TUNEL/sarcomeric actin/DAPI positive myocytes (WT: 3.7%±1.1%; *Hq* 7.7%±1.4%; $P<0.05$; Figure 4A through 4D). *Hq* mice also demonstrated an increase in necrotic cell death, as evidenced by labeling for complement-9/sarcomeric actin/DAPI (WT: 4.9%±0.6%; Hq 15.4%±3.1%; $P<0.05$; Figure 4E through 4H). Together, our data indicate that the AIF-deficient myocardium is highly sensitized to ischemia-reperfusion injury, with a lower sensitivity threshold in older animals. This latter finding is further supportive toward a role

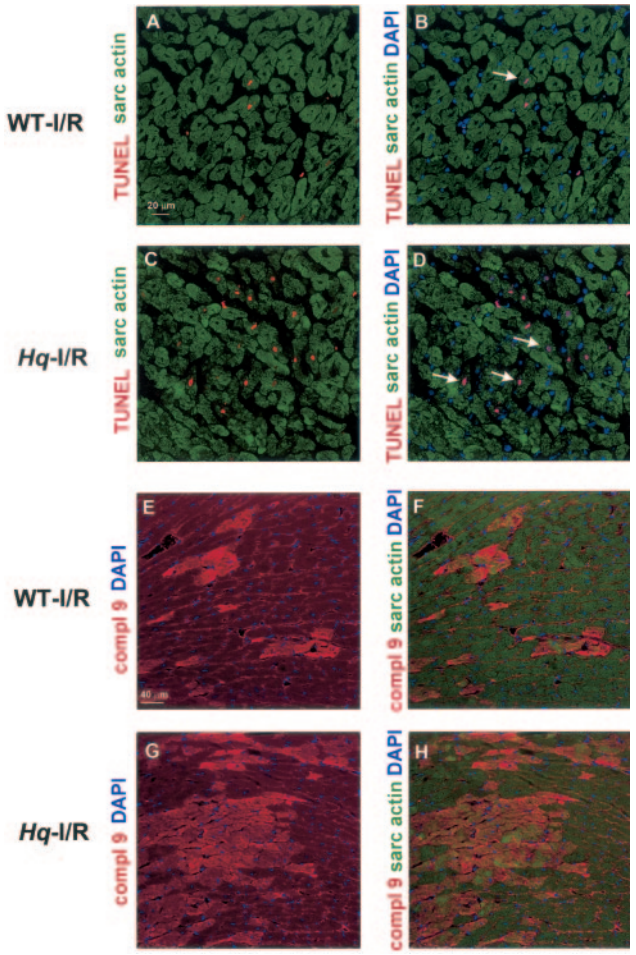

Figure 4. Typical appearance of different types of cell death in I/R-WT and *Hq* hearts. A and C, confocal micrographs of TUNEL-labeled nuclei (red) counterstained for sarcomeric cardiac actin (green). B and D, merged confocal images with TUNEL-labeled myocytes (red), sarcomeric actin (green), and nuclei (blue). Note the higher incidence of TUNEL-positive cardiomyocytes in *Hq* I/R hearts compared with WT I/R hearts. E and G, confocal images of necrotic cells positive for complement 9 (red), counterstained for nuclei (blue). F and H, merged images for complement 9 (red), sarcomeric actin (green), and DAPI (blue), indicate a higher incidence of necrotic cell death in *Hq* hearts subjected to I/R.

for AIF as cardiac antioxidant, as normal senescence is accompanied by changes in the myocardium that decrease its capacity to tolerate and respond to oxidative stress.[30]

AIF Deficiency Promotes Maladaptive LV Remodeling in Response to Biomechanical Stress

Mechanical load activates signaling cascades including oxidative stress,[31] predisposes cardiac muscle to late-onset apoptosis,[1] and can trigger apoptosis acutely, especially in susceptible backgrounds.[32] To test whether downregulation of AIF may sensitize the myocardium to biomechanical stress-induced injury, adult *Hq* and WT mice were subjected to sham operations or TAC to mimic cardiovascular conditions such as aortic valve stenosis and hypertension. Cardiac geometry and function was assessed noninvasively by serial echocardiography at weekly intervals up to 28 days after intervention (Figure 5A).

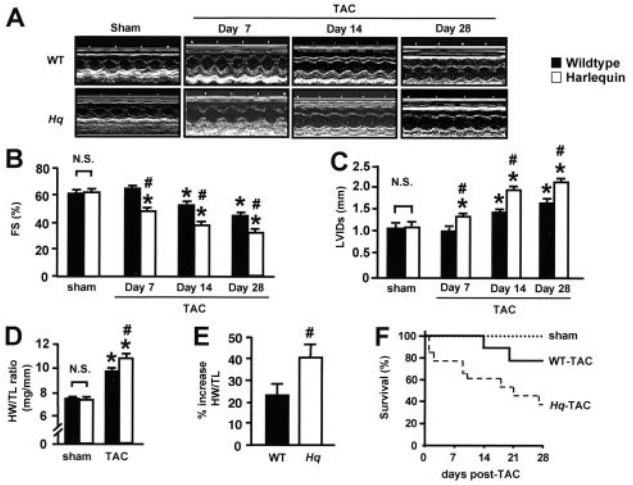

Figure 5. Accelerated LV dysfunction, hypertrophy, and reduced survival in AIF-deficient mice subjected to biomechanical stress. A, Representative M-mode echocardiography images at serial intervals in WT and *Hq* mice, after sham operation, 7, 14, or 28 days after TAC. B, Fractional shortening (FS), a measure of systolic contractility, was similar in sham-operated mutant and WT mice, but was progressively and significantly decreased in *Hq* mutant mice compared with WT mice after 4 weeks of TAC. C, Similarly, systolic left ventricle (LV) internal diameter was similar in sham-operated mutant and WT mice, but increased more pronounced in *Hq* mutant mice after aortic banding, suggesting accelerated and progressive LV dilation compared with WT mice. D, HW/TL ratios increased in both groups after 4 weeks of TAC compared with corresponding sham operated groups, but the percentage increase was more pronounced in *Hq* mutant mice (E), indicating that *Hq* mice have an exaggerated hypertrophy response after mechanical load. F, Kaplan–Meyer curve demonstrates increased TAC mortality in *Hq* mutant mice compared with WT (both sham groups n=4 to 6; WT-TAC n=9; *Hq*-TAC n=12). $^{*}P<0.05$ TAC vs sham; $^{\#}P<0.05$ *Hq* vs WT.

As shown in the Table and Figure 5A through 5C, baseline function and geometry were similar in *Hq* and WT mice. Seven days of pressure overload in WT mice did not affect internal chamber diameters, and there even was a tendency toward increased LV contractility as assessed by % FS. After 4 weeks of TAC, WT mice displayed relatively mild signs of LV decompensation noted by a 28% decrease in FS (sham 59.8%±1.2%; 1-week TAC, 63.7%±1.9%; 2-week TAC, 51.5%±1.7%; 4-week TAC, 43.0%±0.9%; $P<0.05$ TAC versus sham; Table and Figure 5B) and an increase in LV internal diameters (LVIDs; sham, 1.03±0.08 mm; 1-week TAC, 0.90±0.07 mm; 2-week TAC, 1.47±0.04 mm; 4-week TAC, 1.70±0.05 mm; $P<0.05$ TAC versus sham; Table and Figure 5C). In marked contrast, overall contractility and cardiac geometry in *Hq* mice were considerably worse than their WT counterparts already after 7 days of mechanical load and continued to deteriorate as illustrated by a progressive decline in FS (sham, 60.7%±1.2%; 1-week TAC, 47.1%±1.0%; 2-week TAC, 36.8%±1.7%; 4-week TAC, 30.8%±1.0%; $P<0.05$ TAC versus sham; Table and Figure 5B) and progressively increasing LVIDs (sham, 1.03±0.08 mm; 1-week TAC, 1.37±0.05 mm; 2-week TAC, 1.97±0.04 mm; 4-week TAC, 2.12±0.09 mm; $P<0.05$ TAC versus sham; Table and Figure 5C).

As expected after 4 weeks after TAC, WT hearts displayed hypertrophy, but the hypertrophic response of the *Hq* heart was accentuated, as reflected by a near 2-fold higher percent-

age increase in HW/TL ratio compared with WT mice after TAC (WT, 23% versus *Hq*, 36% increase; $P<0.05$; Figure 5D and 5E, data not shown).

Finally, the survival rates of WT and *Hq* mice subjected to biomechanical stress were evaluated up to 4 weeks after TAC. The survival of sham-operated mice in either genotype was 100% after 4 weeks of TAC. Differences in survival became evident in the first week after TAC and further accentuated up to 4 weeks after TAC, with a substantially higher number of *Hq*-TAC mice succumbing suddenly or with clear signs of heart failure. The survival of WT-TAC mice was 100% and 78% at 1 and 4 weeks after surgery, whereas the survivability of *Hq*-TAC mice amounted to 77% and 38% at 1 and 4 weeks after TAC, respectively (Figure 5F). These observations correlate well with the accelerated deterioration of cardiac function/geometry (Figure 5A through 5C), and the exaggerated hypertrophy response in *Hq*-TAC mice compared with WT-TAC mice (Figure 5D and 5E). Taken together, these data indicate that the AIF-deficient myocardium is highly susceptible to biomechanical stress in terms of maladaptive functional, geometric, and hypertrophic remodeling, accompanied with a higher mortality in AIF deficient mice.

Biomechanical Stress Provokes More Oxidative Stress, Cell Death, and Fibrosis in AIF Deficient Myocardium

The oxidative DHE was used to evaluate the production of superoxide. DHE is freely permeable to cells and in the presence of superoxide anions oxidizes to fluorescent ethidium, which is intercalated into the DNA. Fluorescent ethidium is therefore a marker of intracellular superoxide anion generation. At baseline, *Hq* and WT hearts demonstrated equal DHE fluorescence (Figure 6A). However, after TAC both groups showed an increase in production of superoxide anions, which was slightly more pronounced in *Hq* mice (Figure 6A). These data directly demonstrate that mechanical stress, such as aortic banding, leads to a higher oxidative stress.

Next, we performed immunohistochemical analyses on WT and *Hq* cardiac sections to detect the presence of activated (cleaved) caspase-3, a hallmark of apoptosis, which revealed a very low incidence of positive myocytes in both sham groups, a mild increase in apoptotic myocytes in WT-TAC mice, and a dramatic increase in myocyte apoptosis in *Hq* TAC mice (WT sham $0.11\%\pm0.01\%$, *Hq* sham $0.19\%\pm0.02\%$, WT-TAC $0.35\%\pm0.04\%$; *Hq*-TAC $0.73\%\pm0.09\%$; $P<0.01$ *Hq* TAC versus WT TAC; Figure 6B and 6C). Immunohistochemistry using an antibody for cleaved PARP, a late hallmark of apoptosis, confirmed an increased apoptotic rate in *Hq* mice after TAC compared with their WT counterparts (Figure 6D). Next, to more firmly confirm the apoptotic findings, we performed TUNEL labeling on sham and TAC subjected *Hq* and WT hearts, and costained with phalloidin and DAPI to distinguish the cardiac cell types. Figure 6E demonstrates a representative confocal image of a merged TUNEL/phalloidin/DAPI-positive cardiac myocyte. A very low incidence of TUNEL-positive cardiac myocytes was detectable in both sham-operated groups (WT sham $0.028\%\pm0.014\%$, *Hq* sham $0.037\%\pm0.015\%$; N.S.), a slight increase in WT-TAC hearts, and a substantially higher incidence in Hq-TAC hearts (WT TAC $0.179\%\pm0.031\%$, *Hq* TAC $0.346\%\pm0.044\%$; $P<0.05$ versus corresponding sham groups and $P<0.05$ WT-TAC versus *Hq*-TAC; Figure 6F).

As oxidative stress provokes both apoptosis as well as necrosis, the incidence of the latter form of cell death was also evaluated using complement-9/phalloidin/DAPI immunohistochemical labeling and confocal microscopy.[23] Necrotic cell death was a relatively rare phenomenon in sham operated hearts of either genotype, amounting to 0.29 ± 0.02 ‰ in WT-sham hearts and 0.31 ± 0.02 ‰ in Hq-sham hearts (N.S.; Figure 6H). After biomechanical stress, increased numbers of necrotic cells were observed in both groups, however significantly more necrosis was evident in Hq-TAC hearts (0.64 ± 0.04 ‰ in WT-TAC and 0.89 ± 0.04 ‰ in Hq-TAC; $P<0.05$ versus corresponding sham groups, $P<0.05$ WT-TAC versus Hq-TAC; Figure 6H).

H&E staining confirmed increased cross-sectional myofiber size in response to mechanical load in both genotypes but more pronounced in *Hq* mice (WT sham 181 ± 12 μm^2, Hq sham 154 ± 7 μm^2, WT-TAC 339 ± 10 μm^2, Hq-TAC 387 ± 10 μm^2; $P<0.01$; Figure 6I and 6J). Furthermore, pronounced interstitial fibrosis was evident in *Hq* but not WT hearts after TAC (Figure 6I). Collectively, these data demonstrate a predisposition of AIF-deficient mice to develop LV dysfunction, dilation, and increased mortality, coupled to pathological LV remodeling encompassing accentuated oxidative stress, cell death, and fibrosis in response to mechanical load accompanied by oxidative stress.

AIF Functions as a Cardiac Antioxidant Independent of Mitochondrial Complex Activity

To more directly address why the AIF-deficient cardiac muscle is sensitized to oxidative stress, we investigated mitochondrial function in more detail, as increased production of reactive oxygen species can result from respiratory chain (RC) dysfunction and decreased antioxidant mechanisms. Superoxide derives primarily from complex I and III of the RC. Conversely, complex I and IV functioning are readily deteriorated by ROS, which further increases the production of ROS of the RC. Therefore, we measured the RC complexes I and IV in WT and *Hq* hearts, which demonstrated that the enzymatic activities of both complexes were not different between *Hq* and WT (Figure 7A and 7B). To exclude that in *Hq* mouse hearts a potential decrease in the RC complexes has been compensated by an increase in mitochondrial numbers, the level of mitochondrial matrix enzyme citrate synthase was determined as a reflection of the mitochondrial mass.[33] No differences in mitochondrial density were found between both groups (Figure 7C). This indicates that the respiratory chain in *Hq* mutant hearts is fully functional and will not likely underlie a higher rate of superoxide production than in WT hearts.

However, we found that mechanical stress led to higher levels of superoxide in both *Hq* and WT mice, as shown by their increased DHE staining (Figure 6A). The antioxidant enzyme manganese superoxide dismutase (MnSOD) will neutralize superoxide by its conversion into H_2O_2. Immuno-

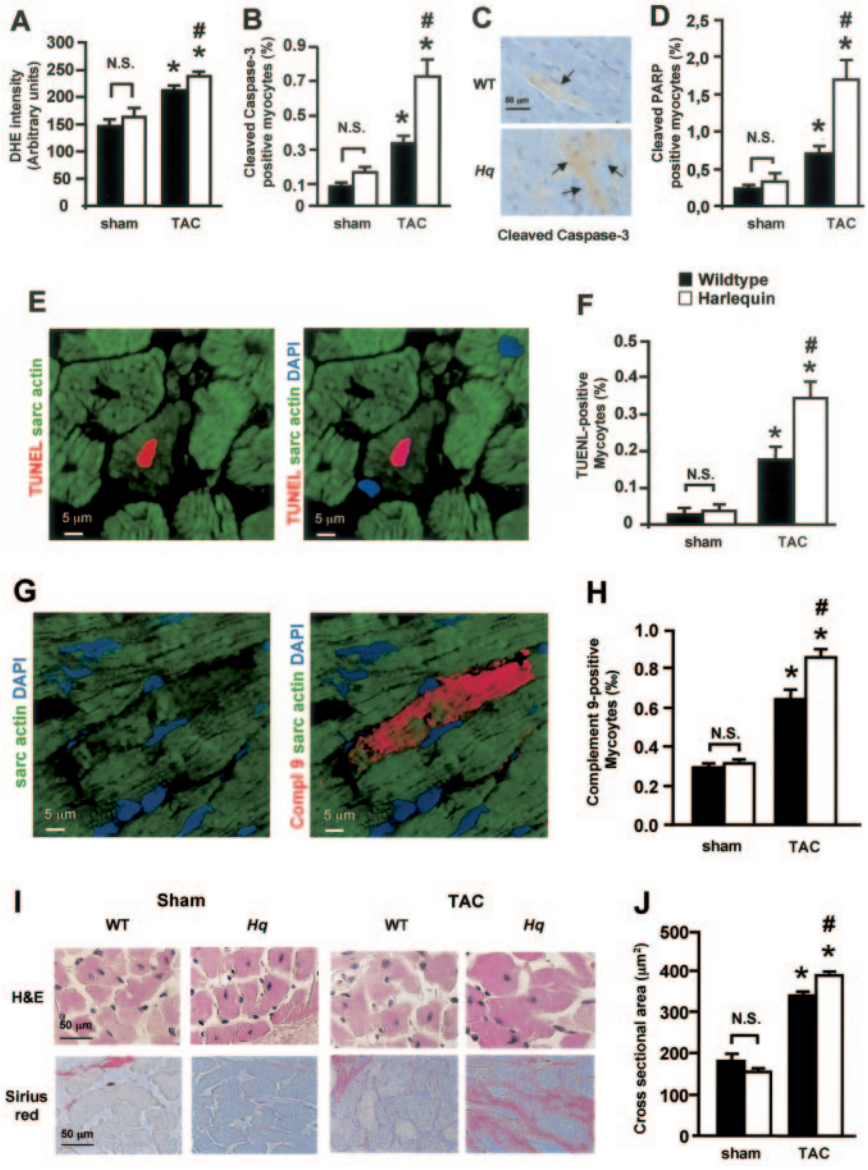

Figure 6. Elevated oxidative stress, elevated cell death, and pronounced fibrosis in AIF-deficient myocardium after biomechanical stress. A, DHE was used to visualize and quantify the production of superoxide in situ. WT and *Hq* mice demonstrated a significantly higher level of superoxide production after aortic banding. B, WT and *Hq* hearts, subjected to 14 days of mechanical load, displayed increased myocyte apoptosis as scored by positivity for cleaved caspase-3. However, the percentage increase in *Hq* mutants was more pronounced. C, Representative image of cleaved caspase-3 positive myocytes in WT and *Hq* mutant mice subjected to TAC (arrows denote individual caspase-3 positive myocytes). D, WT and *Hq* hearts demonstrated increased cleaved PARP positive myocytes after TAC, with the percentage increase in *Hq* mutants being more pronounced compared with WT. E, Single cell confocal image of TUNEL-positive cardiomyocyte labeling in *Hq* hearts after aortic banding, with TUNEL-positive nucleus (red), sarcomeric actin (green), and nuclei counterstained with DAPI (blue). F, Quantification of TUNEL-positive cardiomyocytes in WT and *Hq* hearts demonstrate a higher percentage of TUNEL-positive myocytes after TAC compared with WT.G, Single cell confocal image of complement-9 positive myocyte in *Hq* hearts after aortic banding, with complement 9 (red), sarcomeric actin (green), and nuclei counterstained with DAPI (blue). Note the degradation of sarcomeric structures in the necrotic myocyte. H, WT and *Hq* hearts display a higher level of necrotic myocytes after TAC, but this was more pronounced in *Hq* mice compared with WT. I, Representative H&E images at 400× magnification of WT and *Hq* hearts after sham treatment or 4 weeks of TAC, which demonstrate marked increased in myocyte fiber diameter in *Hq*-TAC mice compared with other experimental groups (upper). Sirius red staining demonstrates prominent fibrosis in *Hq* mice subjected to TAC (lower). J, Quantification of cross-sectional area of myofibers from indicated groups shows an accentuated myocyte hypertrophy response in *Hq*-TAC mice (n=4). $^{*}P<0.05$ vs corresponding sham group; $^{\#}P<0.05$ *Hq* vs WT.

blot analysis demonstrated that the expression of MnSOD was not significantly different between *Hq* and WT mice, indicating an equivalent ability of both mouse strains to handle superoxide (Figure 7D). To investigate whether *Hq* and WT hearts are also able to handle H_2O_2 equally, subsarcolemmal mitochondria were freshly isolated from WT and *Hq* hearts and challenged with 10.5 mmol/L H_2O_2. The data demonstrate a 29% decrease in H_2O_2 clearance rate in *Hq* mitochondria compared with their WT counterparts (WT, 6.0±0.3; *Hq*, 4.3±0.6 µmol/L H_2O_2/min/U CS; Figure 7E). These results directly demonstrate that AIF deficiency decreases the ability of cardiac mitochondria to decompose H_2O_2, which more firmly establishes an antioxidant function for AIF. Taken together, the combined observations suggest that under conditions of increased oxidative stress, AIF deficiency uncovers an inadequate myocardial antioxidant ability that is no longer capable to neutralize the increased ROS production, resulting in increased cell death, myocardial injury, and predisposition to heart failure. The precise biochemical mechanisms by which AIF neutralizes ROS remain to be elucidated and should become the focus of future analyses.

Discussion

Our data demonstrate an important role for AIF in cardiac cell survival both in isolated cultured cardiomyocytes and in the intact heart, although the precise mechanism for AIF protection in these cells is not known. Klein et al posit that AIF could regulate, directly or indirectly, free radical scavenging and thereby help ameliorate hydrogen peroxide–mediated

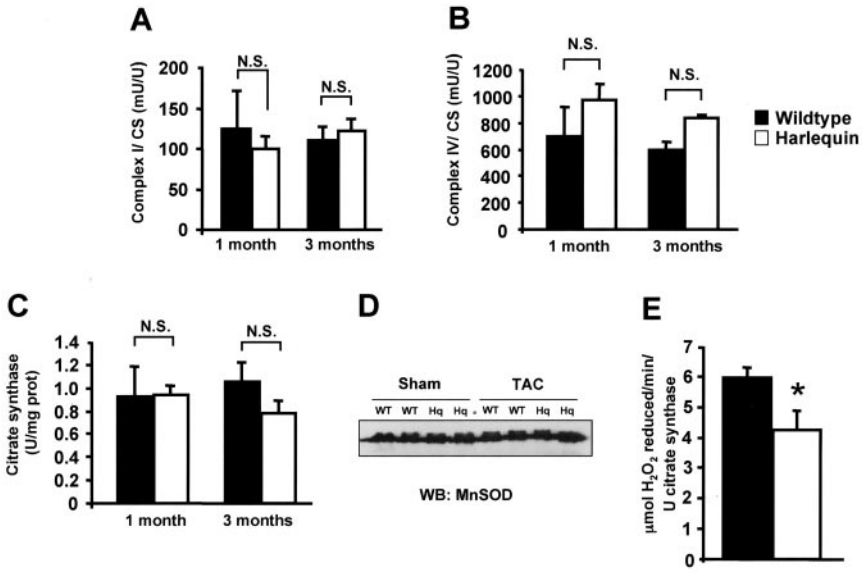

Figure 7. Cardiac mitochondrial function in WT and *Hq* mice. A and B, Measurement of respiratory chain complex I and IV activity in 1-month- and 3-month-old *Hq* and WT mitochondria demonstrated comparable complex I (A) and complex IV function (B). Complex I and IV activity values were standardized for the amount of mitochondria (citrate synthase). C, Citrate synthase assay on hearts of 1- or 3-month-old WT and *Hq* mice indicate no differences in mitochondrial density between the 2 groups. D, Western blot analysis on WT and *Hq* hearts under baseline conditions or subjected to TAC demonstrated no differences in MnSOD expression. E, Mitochondria isolated from 1-month-old WT or *Hq* mice were challenged with 10.5 mmol/L H_2O_2 and their H_2O_2 clearance rate was measured. AIF deficient mitochondria demonstrated a decreased clearance rate compared with their WT counterparts.

apoptosis, but no direct mechanistic evidence for this premise was presented.[14,34] Although AIF does not appear to physically associate with components of the respiratory complex,[35] in theory, it is possible that AIF plays a critical role in mitochondrial respiration, by handling of reactive oxygen radicals that are normally released by the respiratory chain. In fact, a recent study demonstrated loss of complex I activity in *Hq* brain and retina at 10 weeks of age.[35] However, as in the current study, no alterations in respiratory complex activity were observed in *Hq* hearts, a tissue without baseline pathology, nor did we observe an increase in mitochondrial number, which might compensate for respiratory deficiencies. This apparent tissue specificity may be reflective of differences between tissues in assembly of respiratory complexes,[35] or might be the result of the increase in free radical production observed in the CNS.[14]

Alternatively, whereas oxidative phosphorylation is apparently normal in *Hq* hearts, our data demonstrates a deficiency in the scavenging of exogenous H_2O_2 in isolated *Hq* mitochondria. This suggests that AIF itself, or as part of a yet to be determined complex, may have free radical scavenging properties, and as such constitutes a novel cardiac antioxidant that protects the myocardium from oxidative stress under ischemic or biomechanical stress. In agreement, AIF negative cells under stress conditions were found to deplete nonoxidized glutathione more rapidly than cells that expressed AIF, suggesting that AIF is necessary for the maintenance of glutathione levels, at least under some conditions.[36] It is of interest to note the similarity between the oxidoreductase enzyme AIF and the thioredoxin system, consisting of thioredoxin 1 (Trx)1, thioredoxin reductase, and NADPH, which operates as a powerful antioxidant protein–disulfide oxidoreductase system.[37,38] Lowering the antioxidant function of the thioredoxin system in the heart provokes oxidative stress in the cardiac muscle,[31] and predisposes the heart, as does the *Hq* mutation, to cardiac decompensation in response to mechanical load. Whether AIF also has such partners is not known, but the present study shows that the residual AIF in the *Hq* mouse heart apparently suffices to prevent oxidative stress under normal conditions. However, *Hq* mitochondria have a decreased capacity to neutralize a high H_2O_2 challenge, and in response to elevated ROS production from, either exogenous (H_2O_2 administration) or endogenous sources (acute ischemia-reperfusion/biomechanical stress), the free radical scavenging function in *Hq* hearts is clearly inadequate.

Heart failure can be initiated by a plethora of inherited or acquired insults that invariably provoke left ventricular remodeling, which is characterized by elevated levels of myocyte apoptosis. Because of its limited regenerative capacity the heart is exquisitely sensitive to the low, but constant, loss of muscle cells that may precipitate in a progressive loss of functional units and, concomitantly, a loss of contractility. A feature that clearly influences the mitochondrial programmed cell death pathway is oxidative stress evoked by excessive intracellular concentrations of ROS. A large body of studies has elucidated a crucial role for ROS in ischemia/reperfusion-related damage of the heart muscle, and increasing evidence implicates oxidative stress in the progression of heart failure. In fact, intrinsic oxidative stress was demonstrated to increase with age in the heart, because of both age-related impairment of transcriptional responses to oxidant stress,[39] diminished expression of antioxidant defense enzymes such as glutathione peroxidase and MnSOD,[39] and as a result of age-dependent cardiac mitochondrial dysfunction.[40] These age-related effects, coupled to the relatively high dependence of fatty acid β-oxidation of the heart, which holds the risk of lipid peroxide–derived oxygen species formation, may contribute to the higher incidence of cardiovascular disorders such as heart failure in the aged population. Protecting the heart against excessive oxidative stress may, therefore, constitute a bona fide therapeutic device in the prevention of heart failure, stressing the importance to elucidate the factors involved in providing protection against noxious ROS. The findings in our study underscore the importance of ROS in ischemia/reperfusion damage and development of heart failure and implicate a role for AIF in the protection against oxidative stress related myocardial damage.

Acknowledgments

This work was supported by grants 912-04-054, 912-04-017, and 902-19-275 from the Netherlands Organization for Health Research and Development (ZonMW) and the Hein Wellens Foundation (to L.J.D.W.) and AG19358 from the National Institutes of Health (to S.L.A.). V.v.E. was supported by the Dr Dekker MD/PhD program and a travel Fellowship from the Netherlands Heart Foundation (NHS2001D012). A.T.B. was supported by a young investigator's award of the Fondation Bettencourt Schueller. We thank Chiel de Theije for technical assistance, Karen Svenson and technicians for blood chemistry analysis (National Heart, Lung, and Blood Institute programs for Genomic Application; HL 66611, The Jackson Laboratory), and Drs Xiaosong Wang, Beverly Paigen, Jurgen Naggart, and members of the De Windt Laboratory for valuable comments on the manuscript.

References

1. Lorell BH, Carabello BA. Left ventricular hypertrophy: pathogenesis, detection, and prognosis. *Circulation*. 2000;102:470–479.
2. Wencker D, Chandra M, Nguyen K, Miao W, Garantziotis S, Factor SM, Shirani J, Armstrong RC, Kitsis RN. A mechanistic role for cardiac myocyte apoptosis in heart failure. *J Clin Invest*. 2003;111:1497–1504.
3. Zamzami N, Susin SA, Marchetti P, Hirsch T, Gomez-Monterrey I, Castedo M, Kroemer G. Mitochondrial control of nuclear apoptosis. *J Exp Med*. 1996;183:1533–1544.
4. Hu Y, Benedict MA, Ding L, Nunez G. Role of cytochrome c and dATP/ATP hydrolysis in Apaf-1-mediated caspase-9 activation and apoptosis. *Embo J*. 1999;18:3586–3595.
5. Narula J, Pandey P, Arbustini E, Haider N, Narula N, Kolodgie FD, Dal Bello B, Semigran MJ, Bielsa-Masdeu A, Dec GW, Israels S, Ballester M, Virmani R, Saxena S, Kharbanda S. Apoptosis in heart failure: release of cytochrome c from mitochondria and activation of caspase-3 in human cardiomyopathy. *Proc Natl Acad Sci U S A*. 1999;96:8144–8149.
6. Stennicke HR, Jurgensmeier JM, Shin H, Deveraux Q, Wolf BB, Yang X, Zhou Q, Ellerby HM, Ellerby LM, Bredesen D, Green DR, Reed JC, Froelich CJ, Salvesen GS. Pro-caspase-3 is a major physiologic target of caspase-8. *J Biol Chem*. 1998;273:27084–27090.
7. Varfolomeev EE, Schuchmann M, Luria V, Chiannilkulchai N, Beckmann JS, Mett IL, Rebrikov D, Brodianski VM, Kemper OC, Kollet O, Lapidot T, Soffer D, Sobe T, Avraham KB, Goncharov T, Holtmann H, Lonai P, Wallach D. Targeted disruption of the mouse Caspase 8 gene ablates cell death induction by the TNF receptors, Fas/Apo1, and DR3 and is lethal prenatally. *Immunity*. 1998;9:267–276.
8. Martin DA, Siegel RM, Zheng L, Lenardo MJ. Membrane oligomerization and cleavage activates the caspase-8 (FLICE/MACHalpha1) death signal. *J Biol Chem*. 1998;273:4345–4349.
9. Enari M, Sakahira H, Yokoyama H, Okawa K, Iwamatsu A, Nagata S. A caspase-activated DNase that degrades DNA during apoptosis, and its inhibitor ICAD. *Nature*. 1998;391:43–50.
10. Mashima T, Naito M, Noguchi K, Miller DK, Nicholson DW, Tsuruo T. Actin cleavage by CPP-32/apopain during the development of apoptosis. *Oncogene*. 1997;14:1007–1012.
11. Greidinger EL, Miller DK, Yamin TT, Casciola-Rosen L, Rosen A. Sequential activation of three distinct ICE-like activities in Fas-ligated Jurkat cells. *FEBS Lett*. 1996;390:299–303.
12. Communal C, Sumandea M, de Tombe P, Narula J, Solaro RJ, Hajjar RJ. Functional consequences of caspase activation in cardiac myocytes. *Proc Natl Acad Sci U S A*. 2002;99:6252–6256.
13. Daugas E, Susin SA, Zamzami N, Ferri KF, Irinopoulou T, Larochette N, Prevost MC, Leber B, Andrews D, Penninger J, Kroemer G. Mitochondrio-nuclear translocation of AIF in apoptosis and necrosis. *Faseb J*. 2000;14:729–739.
14. Klein JA, Longo-Guess CM, Rossmann MP, Seburn KL, Hurd RE, Frankel WN, Bronson RT, Ackerman SL. The harlequin mouse mutation downregulates apoptosis-inducing factor. *Nature*. 2002;419:367–374.
15. Wang X, Yang C, Chai J, Shi Y, Xue D. Mechanisms of AIF-mediated apoptotic DNA degradation in Caenorhabditis elegans. *Science*. 2002; 298:1587–1592.
16. Lipton SA, Bossy-Wetzel E. Dueling activities of AIF in cell death versus survival: DNA binding and redox activity. *Cell*. 2002;111:147–150.
17. Arber S, Hunter JJ, Ross J Jr, Hongo M, Sansig G, Borg J, Perriard JC, Chien KR, Caroni P. MLP-deficient mice exhibit a disruption of cardiac cytoarchitectural organization, dilated cardiomyopathy, and heart failure. *Cell*. 1997;88:393–403.
18. De Windt LJ, Lim HW, Haq S, Force T, Molkentin JD. Calcineurin promotes protein kinase C and c-Jun NH2-terminal kinase activation in the heart. Cross-talk between cardiac hypertrophic signaling pathways. *J Biol Chem*. 2000;275:13571–13579.
19. Rockman HA, Ross RS, Harris AN, Knowlton KU, Steinhelper ME, Field LJ, Ross J Jr, Chien KR. Segregation of atrial-specific and inducible expression of an atrial natriuretic factor transgene in an in vivo murine model of cardiac hypertrophy. *Proc Natl Acad Sci U S A*. 1991;88:8277–8281.
20. van Eickels M, Grohe C, Cleutjens JP, Janssen BJ, Wellens HJ, Doevendans PA. 17beta-estradiol attenuates the development of pressure-overload hypertrophy. *Circulation*. 2001;104:1419–1423.
21. Van Rooij E, Doevendans PA, Crijns HJ, Heeneman S, Lips DJ, Van Bilsen M, Williams RS, Olson EN, Bassel-Duby R, Rothermel BA, De Windt LJ. MCIP1 Overexpression suppresses left ventricular remodeling and sustains cardiac function after myocardial infarction. *Circ Res*. 2004.
22. Schultz JE, Witt SA, Nieman ML, Reiser PJ, Engle SJ, Zhou M, Pawlowski SA, Lorenz JN, Kimball TR, Doetschman T. Fibroblast growth factor-2 mediates pressure-induced hypertrophic response. *J Clin Invest*. 1999;104:709–719.
23. Kostin S, Pool L, Elsasser A, Hein S, Drexler HC, Arnon E, Hayakawa Y, Zimmermann R, Bauer E, Klovekorn WP, Schaper J. Myocytes die by multiple mechanisms in failing human hearts. *Circ Res*. 2003;92:715–724.
24. Srere PA. Citrate synthase. *Methods Enzymol*. 1969;13:3–11.
25. Birch-Machin MA, Turnbull DM. Assaying mitochondrial respiratory complex activity in mitochondria isolated from human cells and tissues. *Methods Cell Biol*. 2001;65:97–117.
26. Palmer JW, Tandler B, Hoppel CL. Biochemical properties of subsarcolemmal and interfibrillar mitochondria isolated from rat cardiac muscle. *J Biol Chem*. 1977;252:8731–8739.
27. Bermeyer H. Zur messung von katalase-aktivitaten. *Biochem Z*. 1955; 327:255–258.
28. Chen M, Zsengeller Z, Xiao CY, Szabo C. Mitochondrial-to-nuclear translocation of apoptosis-inducing factor in cardiac myocytes during oxidant stress: potential role of poly(ADP-ribose) polymerase-1. *Cardiovasc Res*. 2004;63:682–688.
29. Xiao CY, Chen M, Zsengeller Z, Li H, Kiss L, Kollai M, Szabo C. Poly(ADP-ribose) polymerase promotes cardiac remodeling, contractile failure and translocation of apoptosis-inducing factor in a murine experimental model of aortic banding and heart failure. *J Pharmacol Exp Ther*. 2004.
30. Powers SK, Quindry J, Hamilton K. Aging, exercise, and cardioprotection. *Ann N Y Acad Sci*. 2004;1019:462–470.
31. Yamamoto M, Yang G, Hong C, Liu J, Holle E, Yu X, Wagner T, Vatner SF, Sadoshima J. Inhibition of endogenous thioredoxin in the heart increases oxidative stress and cardiac hypertrophy. *J Clin Invest*. 2003; 112:1395–1406.
32. Hirota H, Chen J, Betz UA, Rajewsky K, Gu Y, Ross J Jr, Muller W, Chien KR. Loss of a gp130 cardiac muscle cell survival pathway is a critical event in the onset of heart failure during biomechanical stress. *Cell*. 1999;97:189–198.
33. Gabeler EE, Sluiter W, van Hillegersberg R, Edixhoven A, Schoonderwoerd K, Statius van Eps RG, van Urk H. Aminolaevulinic acid-induced protoporphyrin IX pharmacokinetics in central and peripheral arteries of the rat. *Photochem Photobiol*. 2003;78:82–87.
34. Klein JA, Ackerman SL. Oxidative stress, cell cycle, and neurodegeneration. *J Clin Invest*. 2003;111:785–793.
35. Vahsen N, Cande C, Briere JJ, Benit P, Joza N, Larochette N, Mastroberardino PG, Pequignot MO, Casares N, Lazar V, Feraud O, Debili N, Wissing S, Engelhardt S, Madeo F, Piacentini M, Penninger JM, Schagger H, Rustin P, Kroemer G. AIF deficiency compromises oxidative phosphorylation. *Embo J*. 2004.
36. Cande C, Vahsen N, Metivier D, Tourriere H, Chebli K, Garrido C, Tazi J, Kroemer G. Regulation of cytoplasmic stress granules by apoptosis-inducing factor. *J Cell Sci*. 2004;117:4461–4468.
37. Nakamura H, Nakamura K, Yodoi J. Redox regulation of cellular activation. *Annu Rev Immunol*. 1997;15:351–369.
38. Masutani H, Yodoi J. Thioredoxin. Overview. *Methods Enzymol*. 2002; 347:279–286.
39. Edwards MG, Sarkar D, Klopp R, Morrow JD, Weindruch R, Prolla TA. Age-related impairment of the transcriptional responses to oxidative stress in the mouse heart. *Physiol Genomics*. 2003;13:119–127.
40. Lucas DT, Szweda LI. Cardiac reperfusion injury: aging, lipid peroxidation, and mitochondrial dysfunction. *Proc Natl Acad Sci U S A*. 1998; 95:510–514.

Supplemental Table I
Blood chemistry analysis in 6 month old WT and *Hq* mice

	WT	*Hq*
n	16	18
Red Blood Cell Count, 10^6 cells / μ l	9.41 ± 0.09	9.32 ± 0.12
Measured Hgb, g/dL	13.8 ± 0.2	13.7 ± 0.2
Mean Cell Hemoglobin Concentration, g/dL	36.5 ± 0.2	36.5 ± 0.1
Mean Cell Volume, fL	40.3 ± 0.2	40.2 ± 0.2
% Reticulocyte	1.87 ± 0.06	1.79 ± 0.10
Platelet Count, 10^3 cells / μ l	889 ± 38	898 ± 46
Partial Thromboplastin Time, sec	26.0 ± 0.7	24.8 ± 0.4
Prothrombin Time, sec	11.3 ± 0.1	10.8 ± 0.1
White Blood Cell Count, 10^3 cells / μ l	8.2 ± 0.5	13.7 ± 0.2 *
% Lymphocyte	82.9 ± 1.4	78.5 ± 1.6
% Monocyte	1.21 ± 0.1	1.63 ± 0.18
% Neutrophil	12.9 ± 1.3	16.1 ± 1.5
% Basophil	0.54 ± 0.04	0.52 ± 0.04
% Eosinophil	2.15 ± 0.12	2.91 ± 0.25
Glucose SS other, mg/dL	176 ± 7	166 ± 6
Total Cholesterol, mg/dL	80.6 ± 5.8	76.2 ± 4.1
HDL Cholesterol, mg/dL	69.2 ± 5.8	65.6 ± 4.2

Data are expressed as mean ± SEM; * indicates $P < 0.05$ vs WT